Special Issue Article

Institution of MECHANICAL ENGINEERS
Journal of POWER AND ENERGY

Proc IMechE Part A:
J Power and Energy
227(6) 683–691

DOI: 10.1177/0957650913498736
pia.sagepub.com
SAGE

An advanced axial-slot casing treatment on a transonic compressor: A close look with computational fluid dynamics and experimental validation

JA Streit[1], C Brandstetter[2], F Heinichen[3] and H-P Kau[1]

Abstract

The numerical and experimental investigation of non-axisymmetric casing treatments is complex compared to axisymmetric ones like circumferential grooves. Hence they are still rarely investigated, at least regarding combinations of numerical and experimental work on the same configuration. The casing treatment under investigation is capable of significantly broadening the operating range of a tip-critical transonic compressor. This is accomplished without an efficiency penalty at design conditions. It is demonstrated that the application of a casing treatment over the rotor might impose negative effects on the downstream stator that would have to be considered in future designs. Earlier work by the authors was focused on the experimental investigation, in particular of transient effects near stall. In this paper, RANS and URANS simulations are presented in detail. These are used to further study and explain the causes of the effects that were found experimentally. Additional experimental data are added where appropriate, continuing the validation of the numerical methods.

Date received: 29 May 2013; accepted: 5 June 2013

Introduction

The transonic compressor used for the present investigations is representative of the high-pressure compressor front stage of a modern jet engine. It was designed to be tip-critical, so that compressor stall emerges from the rotor tip, making it particularly suitable for the application of casing treatments (CTs).[1] The experimental setup was described by Brandstetter et al.[2]

The CT was developed as part of a past project at the Institute for Flight Propulsion of TU München. It is similar to the ones used by Hembera et al.[3] and Johann and Heinichen.[4] The specific shape of the axial slots enables a grand stall margin extension whilst maintaining or even slightly increasing efficiency at design conditions.

There has been experimental investigation of this specific type of CT over a transonic compressor rotor within a multistage rig.[4] But the critical blade row in the multistage setup was one of the downstream subsonic ones.[4] Thus, the amount of surge margin improvement enabled by the CT could not be verified for the transonic case.

Modification of the rotor geometry is the long-term goal of the research project. This requires an understanding of the CT effects on the main passage flow. Additionally, effects on downstream blade rows will be discussed because a positive influence on the rotor might be counteracted by effects on the stator performance.

Test case and numerical setup

A characteristic of the 1.5-stage compressor without CT at design speed was calculated with steady-state RANS computations. A description of the code used was provided by Lapworth.[5] Calculations were performed with a Spalart–Allmaras turbulence model, automatically applying wall functions depending on a y^+ criterion. The model for the steady-state computations consisted of one blade passage each of inlet guide vane (IGV), rotor and stator, as well as an inflow duct (see Figure 1(a)). All parts were connected using mixing plane interfaces. A radial equilibrium boundary condition with specified static pressure at the hub was applied at the stator exit.

[1]Institute for Flight Propulsion, Technische Universität München, Garching, Germany
[2]Institute for Gas Turbines and Aerospace Propulsion, Technische Universität Darmstadt, Darmstadt, Germany
[3]Rolls-Royce Deutschland, Dahlewitz, Germany

Corresponding author:
JA Streit, Institute for Flight Propulsion, Technische Universität München, Boltzmannstr. 15, 85748 Garching, Germany.
Email: streit@lfa.mw.tum.de

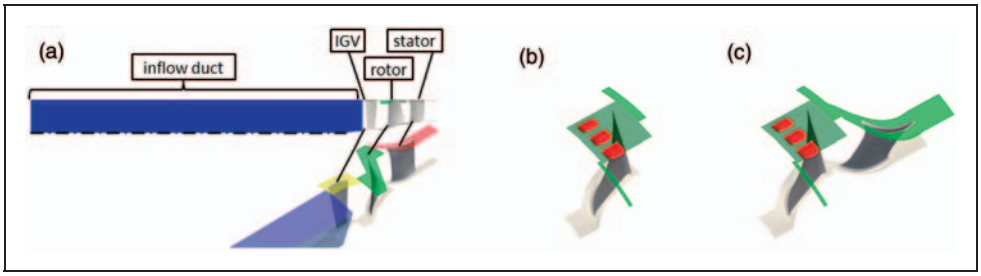

Figure 1. Computational domains. (a) For steady-state simulations of whole 1.5 stages. (b) For unsteady simulations, scaled CT and (c) For unsteady simulations, scaled CT plus stator.
IGV: inlet guide vane.

Unsteady simulations of the 1.5 stages in their entirety would be very demanding on computational power. To decrease computational demands, reduced 'rotor-only' models were developed to enable the simulation of a variety of operating points with the CT to foster the understanding of the CT/rotor flow interaction.

At first, the rotor row was isolated. Here the original spacing was used for the CTs. The boundary conditions were of 'non-reflecting' type[6] for the inlet and outlet and derived from the results of the steady-state simulations of the whole 1.5-stage compressor. The inlet conditions were defined in the stationary frame of reference at the IGV exit, while a prescribed static pressure profile was assigned to the rotor outlet. The axial slots were modeled on a thin patch in the stationary frame of reference. The patch was connected to the rotor casing by a sliding plane interface. In a subsequent study, the model was further reduced in size by applying domain scaling to the CT to enable calculations with only one rotor passage (see Figure 1(b)). To preserve casing porosity, the CTs were narrowed in the circumferential direction. It was shown that the global influence of the CT on the rotor performance was in compliance with that for the larger model, even though the timing between the rotor and CT changed. This is in agreement with the observations of Schnell et al.[7] who performed a study on a similar amount of scaling with an axial slot CT on a transonic compressor. To assess the influence of the CT over the rotor on the downstream stator, the setup depicted in Figure 1(c) has one single stator passage connected to the rotor domain by a mixing plane interface. Though this interface cancels out unsteady effects on the stator, it still offers an insight into the dominant effects with reasonable computational effort.

Grid sensitivity analysis was performed on three grid levels for the rotor and the CT. They were found to be well within the asymptotic range. The CT grid consists of ~150,000 cells for each slot. The rotor grid consists of ~2.3 million cells per passage. The latter number is composed of 90 cells in the radial, 110 cells in the circumferential and 195 cells in the axial direction. The same rotor grid was used for the steady-state simulation of the full 1.5 stages. For that, the remaining cell numbers are: ~0.2 million for the inflow duct, ~1.8 million for the IGV and ~0.5 million for the stator. The high number for the IGV results from the penny gaps whilst the fixed stator does not feature any gaps.

Stall mechanism without CT

To ensure that the compressor and its numerical representation, respectively, are optimally suited for the application of a CT, the stall mechanisms of the stage without the axial slots were evaluated. For this purpose, it is shown in the following section that the rotor itself is tip-critical and the specific stall mechanism is discussed. In advance, the rotor was checked to be the critical blade row of the compressor, both in simulations and experiments. Results presented in this section were obtained from steady-state simulations with the 1.5-stage model (cf. Figure 1(a)).

Stall mechanism of the rotor

To decide whether the rotor is suitable for the application of a CT of axial-slot type it is vital to understand the stall mechanisms of the rotor. Generally, CTs are especially effective for tip-critical rotors.[1] Thus, it is to be shown first that compressor stall emerges from the rotor tip region. This is done by means of the following numerical results.

Figure 2 shows rotor loss loops on several individual span positions. A significant increase in losses when approaching stall (rising relative inflow angle β_1) points to a full utilization of the operating range. This is visible only for the span positions close to the casing. Thus the tip region seems to reach the stability limit before the lower sections. The small operating range in the relative inflow angle β_1 is typical for a transonic rotor (see Bölcs and Suter[8] p. 115ff). The lower sections do not experience a broader range of relative inflow angles which they could probably handle since they are subjected to subsonic inflow at their radial positions.

After locating the stall inception close to the casing, the specific mechanism is of interest since this is decisive for selecting the type of CT. Figure 3 shows the distribution of the axial velocity component at 96% span, illustrating areas of stagnation and

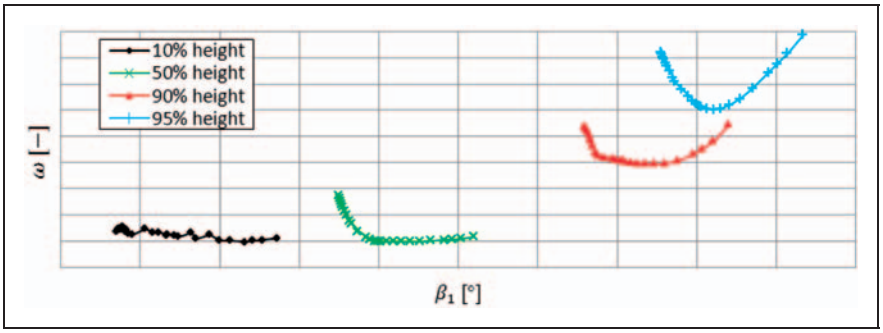

Figure 2. Rotor loss loops on individual relative span positions. All data in relation to values at design operating point and 50% span.

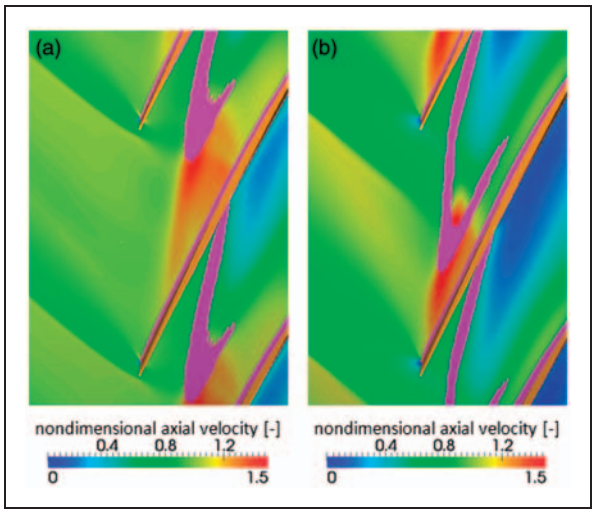

Figure 3. Axial velocity at 96% span. Magenta: areas of high entropy production. (a) Design point and (b) Near stall.

reverse axial flow. Additionally, areas of high entropy creation are depicted in magenta. This way the extent of the tip gap vortex is visible because the highest losses at the considered span position are the mixing losses among the main flow and the vortex.

For the operating point close to stall, the extent of the tip vortex rapidly increases after passing the passage shock. A stagnation area is visible in the core of the vortex as a dark blue area in Figure 3(b). This is presumably the result of a vortex breakdown caused by the vortex–shock interaction. In short, this breakdown is triggered because the low-axial momentum and low-pressure fluid in the vortex core has too low momentum to pass the shock and thus loses its axial velocity, forming the stagnation area. When further throttling the compressor this stagnation area eventually blocks the main passage flow, causing the compressor stall. This mechanism of stall inception in transonic compressors was explained, for example, by Schlechtriem and Lötzerich.[9] For design operating conditions, the faster main passage flow re-energizes the vortex fluid by mixing so that it passes the shock. Additionally, the shock is located further downstream for design conditions giving a longer distance for this mixing process.

Numerical results with CT

Results presented in this section were obtained using the setups with a scaled CT as shown in Figure 1(b) and (c). The smooth casing (SC) calculations were performed with the respective setups, featuring the same casing patch connected via a sliding plane interface but without the actual axial slots. They were calculated by means of steady-state simulations, since a preliminary study showed that transient effects are negligible for the configurations without CT.

Global performance measures

Figure 4 shows the compressor map for the 'rotor-only' setup with the CT compared to the results obtained with a smooth casing. Note that each operating point for the unsteady calculations is actually an accumulation of 12 points representing the time-dependent solutions extracted over one blade passing period. The extension of the rotor's operating range caused by application of the CT is as much as 60% in mass flow. No significant effect of the CT is identifiable at design point (DP) operating conditions. It is noteworthy that no additional penalty in efficiency is generated by the CT, an effect often associated with such a measure.[10] With further throttling of the compressor, a positive influence of the CT on the rotor's efficiency becomes apparent. Along with the improvement in efficiency, the total pressure ratio rises as well.

Unsteady CT flow interactions

The pulsed recirculation flow through one of the axial slots and its result on loss generation in the main flow is illustrated in Figure 5. This is done exemplarily for the operating point corresponding to the near stall point for the smooth casing configuration (NSSC). The single time steps depicted show the unsteady flow pattern through the slot. Fluid from the passage flow between the passing rotor blades is drawn into the downstream part of the slot and reinjected upstream of the blade leading edge. Though the shape of the axial slots lowers the mixing losses at

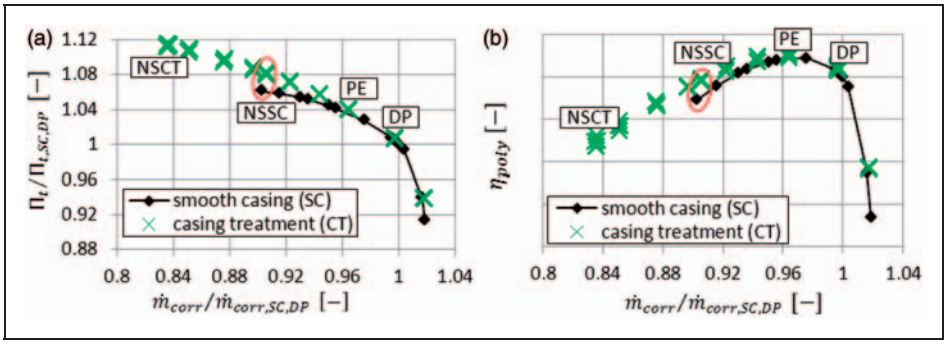

Figure 4. Compressor maps for unsteady 'rotor-only' setup (one rotor blade and three casing slots) compared to results for smooth casing. (a) Total pressure ratio and (b) polytropic efficiency.
NSCT: near stall casing treatment; NSSC: near stall smooth casing; PE: peak efficiency; DP: design point.

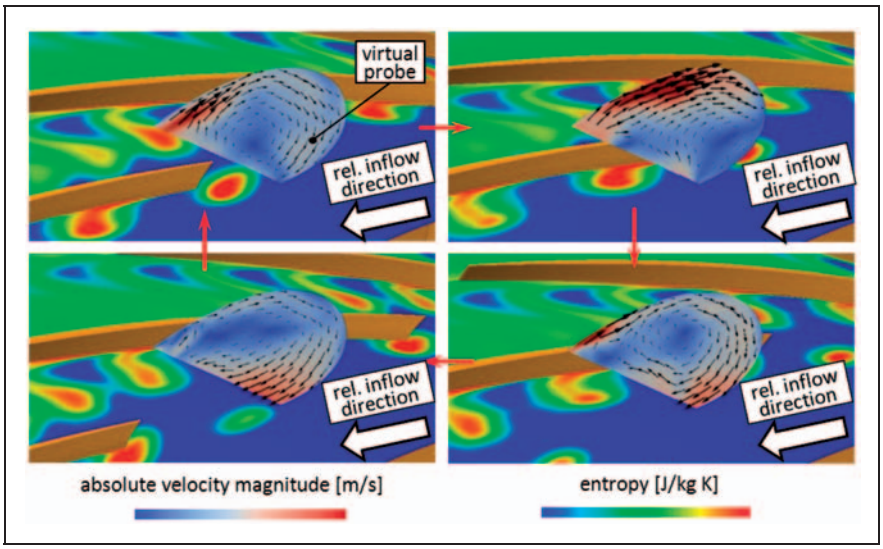

Figure 5. Absolute velocity in axial slot and entropy at 96% span. Operating point NSSC. Red arrows show chronology.

reinjection, these losses are still clearly visible as entropy spots.

To quantify the recirculation in the CT slots and to provide a valuable mean for validation of the numerical model, Figure 6 shows the velocity in the CT for the four operating points marked in the compressor map above. The virtual probe (see Figure 5) used to extract the numerical data was located at the same location as a hot wire probe in the experimental setup.[2] As visible in Figure 5 the high-velocity spots in the slots are very small. Thus to give an exact match of the numerical and experimental data, the numerics not only would have to correctly predict the velocity magnitude but also the exact location of the occurrence of this velocity. Considering this, the numerical predictions show an excellent agreement with the experimental data for PE and NSSC conditions. For design operating conditions, the agreement is still reasonably good. When further throttling the compressor to NSCT, the numerically predicted velocity rises further. This is inconsistent with the experimental data, which unexpectedly shows lower velocity magnitudes at this operating point.

To show that the stall mechanism is effectively tackled by the CT, Figure 7 shows a comparison of the SC and CT setups. The relative velocity magnitude is depicted at 96% span, together with the areas of high entropy production as before. For design operating conditions (Figure 7(a)) hardly any effect of the CT is recognizable. This is consistent with the assumed mode of action of the CT since there is no stagnation area to be drawn off.

Figure 7(b) shows the respective comparison for NSSC. The characteristic shape of the entropy production area vanishes with the application of the CT. It is replaced by a strongly pulsating zone of entropy production that is no longer forked around a stagnation area. As above in static entropy, the additional losses generated by the reinjection of the pulsating CT flow are visible as entropy creation spots at the

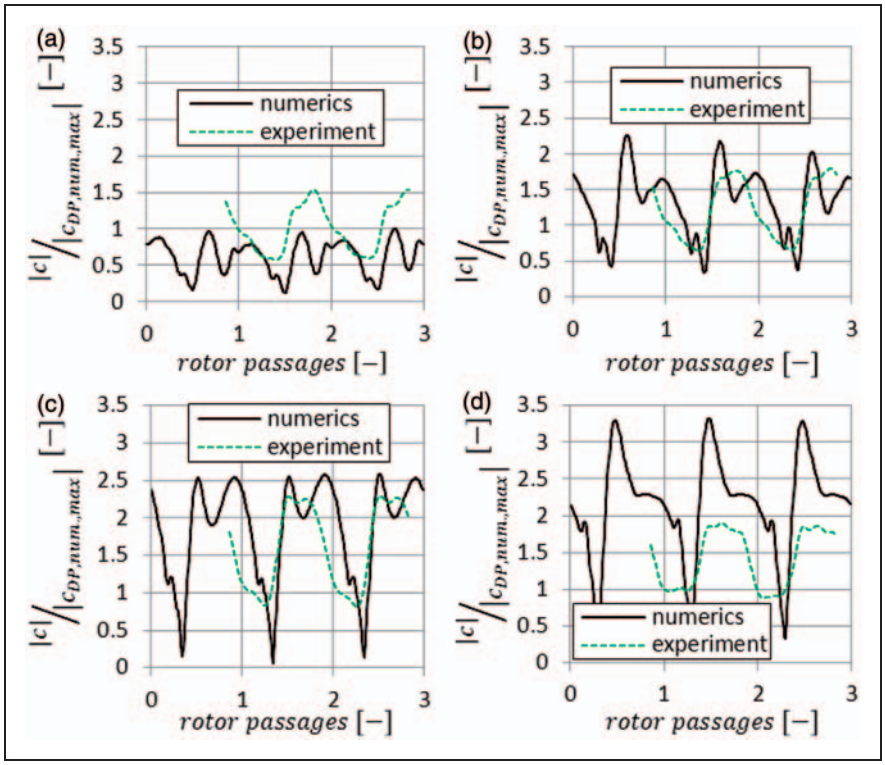

Figure 6. Velocity magnitude in casing treatment at position of hot wire probe: numerical and experimental results. All data in relation to maximum value of numerical results at design point.

upstream end of the slots. These spots move downstream with the main flow, eventually hitting the leading edge of the rotor. Removing the stagnation area and thus increasing the relative Mach number (along with the relative velocity) enables the reduction of the shock detachment from the leading edge as highlighted by the black arrows in Figure 7(b). This downstream movement of the shock lengthens the distance for re-energizing the vortex fluid, thus additionally stabilizing the flow before it passes the shock.

Further throttling of the compressor to the last stable operating point with CT (NSCT) results in the illustration of Figure 7(c). There are no major changes compared with the operating point discussed last. There is still no stagnation area caused by the breakdown of the tip gap vortex. This implies that another mechanism or rather another span position is limiting the aerodynamic stability with the CT.

Figure 8 shows rotor loss loops on individual span positions for the smooth wall and CT setups. Instead of the total pressure loss coefficient, the static entropy rise over the blade row is used to identify losses. The stationary axial slots perform work in the rotor's relative reference system which impacts relative total pressure. Hence, usage of the total pressure loss in the relative coordinate system would produce misleading results.

At 95% span, the CT increases the losses almost over the whole operating range. This can be explained with the mixing losses at injection of the recirculated fluid. At 90% span, the loss reduction introduced by the CT is visible. The operating range is slightly broadened in terms of the relative inflow angle at both span positions.

At span positions close to the hub and at mid-span (10% and 50%), there is no influence of the CT in terms of loss production. But the operating range is significantly increased in these sections. This is in compliance with the blade load reserves on the subsonic sections found experimentally (cf. Brandstetter et al.[2]). For the SC setup, this is not fully utilized because of the critical blade tip. It is no longer possible to identify the critical span position with this simple method, but the above discussion of the tip flow phenomena implies that it is no longer the tip region after application of the CT, but rather a section at about mid-span.

The following discussions of flow phenomena are focused on the stable operating range of the smooth wall configuration where comparisons between that and the setup with CT are possible. The following radial distributions of aerodynamic quantities consider the operating points DP and NSSC. Results with CT are shown as differences to or factors of the corresponding results for the SC setup.

The injection of the recirculated fluid increases the axial momentum of the boundary layer at the casing, see Figure 9. This forces a radial redistribution of mass flow which yields a corresponding reduction of

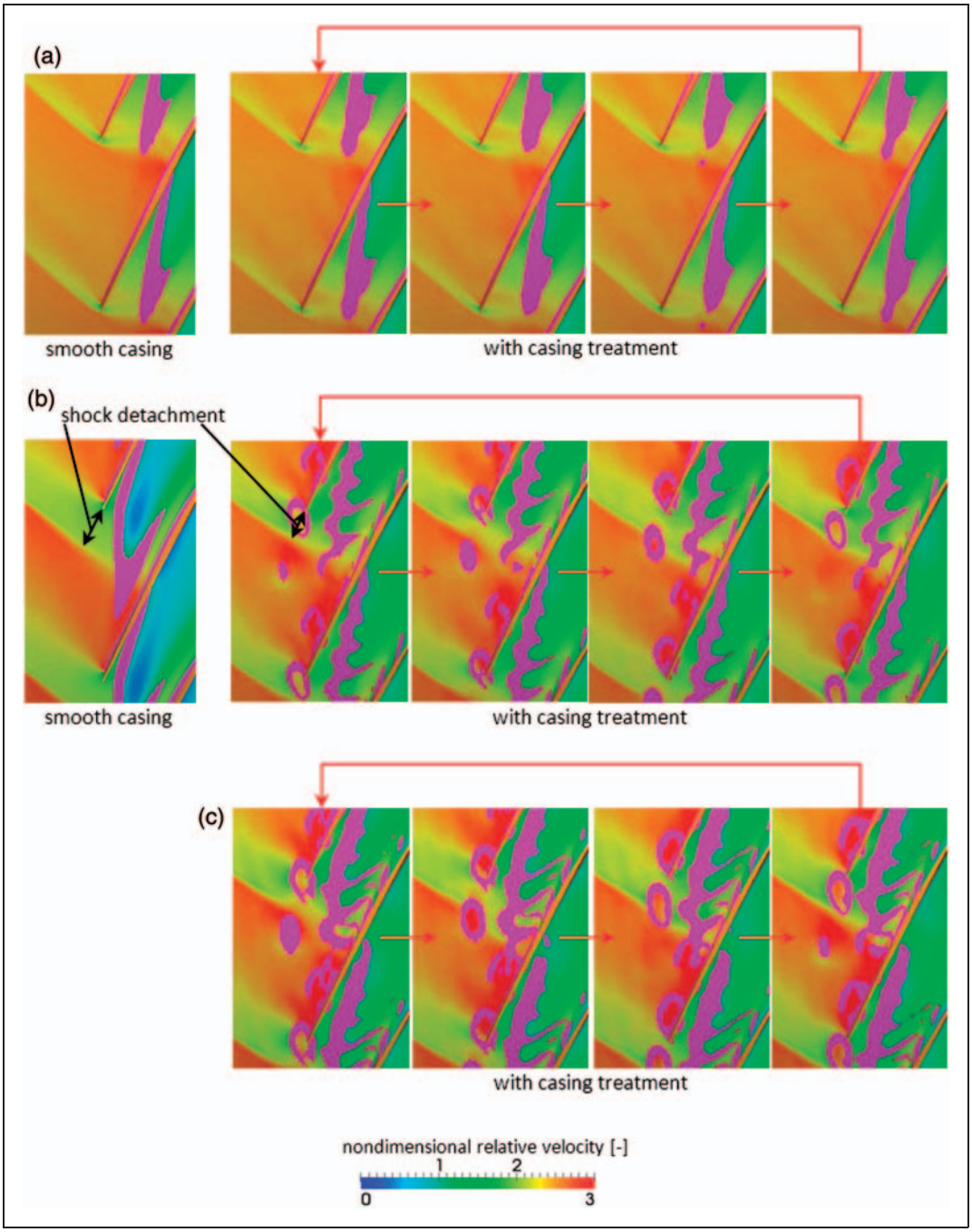

Figure 7. Relative velocity magnitude at 96% span. Magenta: areas of high entropy production. Red arrows show chronology. Representation in relative coordinate system. (a) Design point (DP), (b) Near stall (NSSC) and (c) Near stall (NSCT).

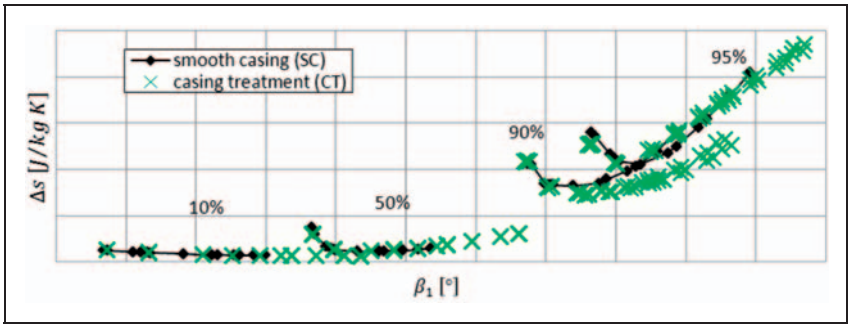

Figure 8. Rotor loss loops on individual span positions: results for smooth casing and with casing treatment.

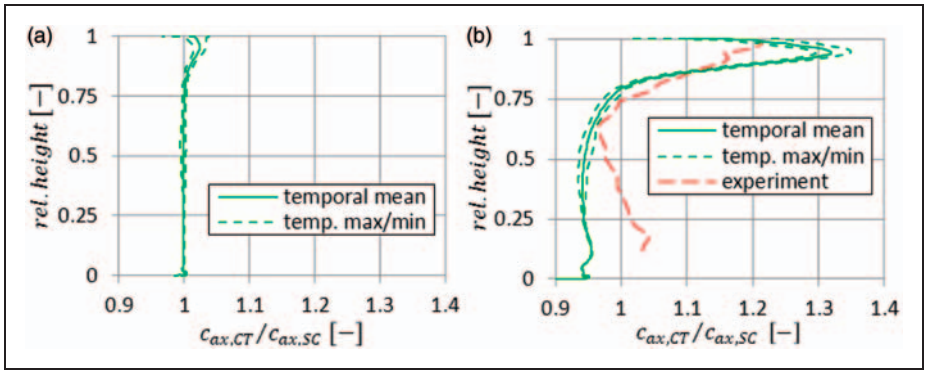

Figure 9. Radial distribution of axial velocity component: results with casing treatment in relation to results with smooth casing. Near stall operating point includes experimental data. (a) Outflow, DP and (b) Outflow, NSSC.

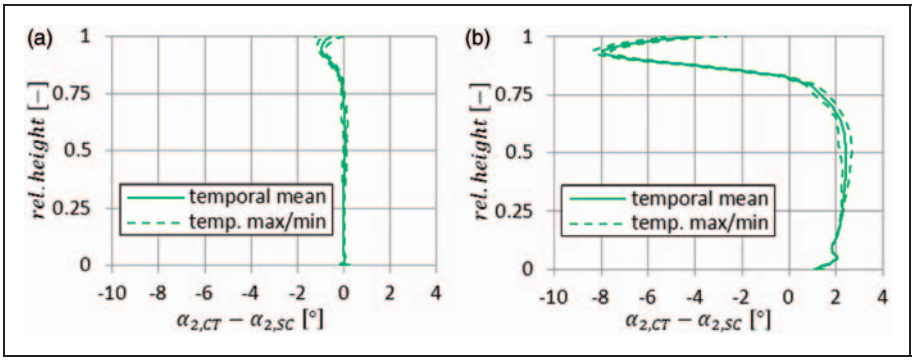

Figure 10. Radial distribution of absolute flow angles: results with casing treatment as deviation from results with smooth casing. (a) Outflow, DP and (b) Outflow, NSSC.

the axial velocity on all lower span positions. Figure 9(b) additionally includes experimental data for the NSSC operating point. The deviations of the numerical data from the experiment are caused by the selection of the outflow boundary condition for the 'rotor-only' numerical setup. This does not entirely correctly represent the influence of the downstream stator on the rotor in the hub region. But in the area above mid-span, which is the focus of interest for the CT effects, the numerical results are in good agreement with the experiment.

The reduction of the axial velocity together with an only marginal increase in relative outflow angle below approximately 75% span yields the radial distributions of absolute outflow angles depicted in Figure 10.

Influence on the downstream stator blade row

The absolute rotor outflow angles shown above are equivalent to the inflow angles for the downstream stator. Positive deviations in these angles represent an increased incidence for the stator. The incidence does not change with the CT at design operating conditions but increases by $\Delta\alpha_2 \approx 2^\circ$ for the throttled operating point (NSSC). Hence, the stator has to offer an operating range broadened by 2° just to enable the same stall mass flow as without the CT. To assess the ability for this of the existing stator, calculations were performed with the setup shown in Figure 1(c). Figure 11 shows the compressor map for these simulations together with the results discussed in the previous section. To enable comparability, the performance data were extracted over the rotor domain only. It is apparent that the most notable effect of the CT, namely the extended operating range, is lost. On the contrary, numerical stall is observed at a higher mass flow rate than without the CT.

Figure 12 shows a separation bubble of increased size for the simulation with CT on the suction side of the stator – typically caused by a too high incidence for the blade – for the NS operating point NSCT*. This indicates the numerical prediction of an aerodynamic overloading of the stator, eventually making the stator the critical blade row. This phenomenon associated with the application of a CT was similarly identified by Madden and West.[11] Since the experiments do not show this strong effect, the simulations seem to overpredict it. Nevertheless, it is a strong indication that the introduction of a CT over the rotor can have a negative influence on the downstream stator. This could yield a penalty in

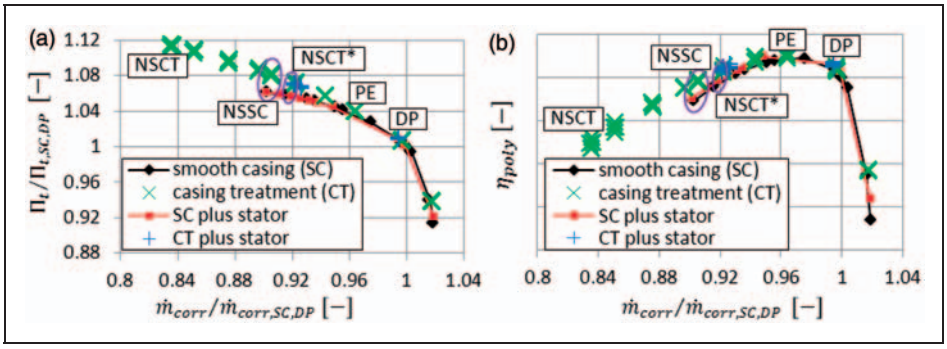

Figure 11. Compressor maps for unsteady 'rotor-only' setup compared to results for SC. Additionally setup with downstream stator, likewise only rotor performance evaluated. (a) Total pressure ratio and (b) polytropic efficiency.
NSCT*: numerical stall point with stator and casing treatment over the rotor; NSCT: near stall casing treatment; NSSC: near stall smooth casing; PE: peak efficiency; DP: design point.

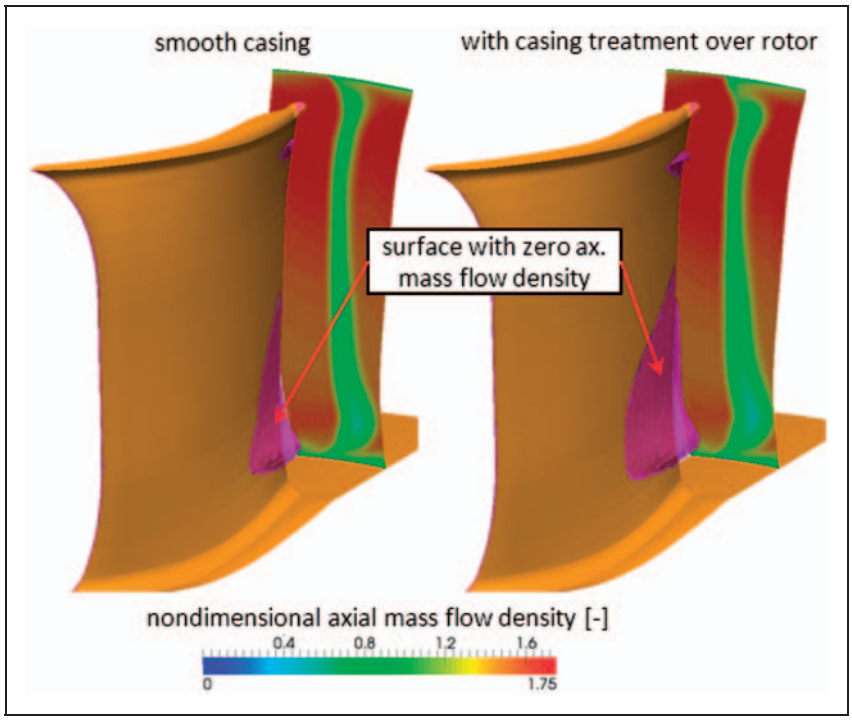

Figure 12. Axial mass flow density at stator exit. Operating point NSCT* is temporal mean of unsteady simulation.
NSCT*: numerical stall point with stator and casing treatment over the rotor.

overall stage efficiency and has to be considered for specific designs incorporating a CT.

Conclusions

The investigated CT is capable of extending the operating range of a tip-critical transonic compressor rotor. Through the geometric shape of the axial slots, this is accomplished without an efficiency penalty at design operating conditions. The stall mechanism of the compressor rotor is the breakdown of the tip leakage vortex interacting with the passage shock. The resulting stagnation area blocks the main passage flow. The main function of the CT is to draw off this stagnation fluid. By removing the stagnation area, the relative velocity in the shroud area is increased, resulting in a repositioning of the passage shock when introducing the CT.

Through the radial redistribution of mass flow in the main passage by the CT, the downstream stator has to handle an extended range of incidence angles. This might lead to flow instabilities or at least to additional losses in the stator which could counteract the beneficial effect of the CT.

The paper points out the potential of the proposed CT geometry. By successfully validating the numerical methods, the foundations are laid for the prospective design of even more efficient CT/rotor combinations.

Acknowledgments

The authors express their gratitude to all the partners involved in the success of this project.

Funding

The investigations presented in this paper were conducted within the German collaboration program 'AG Turbo COORETEC 1.2.3' and were funded by Rolls-Royce Deutschland Ltd. & Co. KG and the Bundesministerium für Wirtschaft und Technologie.

Conflict of interest

None declared.

References

1. Greitzer EM, Nikkanen JP, Haddad DE, et al. A fundamental criterion for the application of rotor casing treatment. *ASME J Fluids Eng* 1979; 101: 237–243.
2. Brandstetter C, Streit JA, Wartzek F, et al. An advanced axial-slot casing treatment on a tip-critical transonic compressor rotor part 1: unsteady hot wire and wall pressure measurements: ETC Paper A070. In: *10th European turbomachinery conference,* Lappeenranta, Finland, 2013.
3. Hembera M, Kau H-P and Johann E. Simulation of casing treatments of a transonic compressor stage: Isromac12-2008-20042. In: *The 12th international symposium on transport phenomena and dynamics of rotating machinery,* Honolulu, HI, 2008.
4. Johann E and Heinichen F. Back to back comparison of a casing treatment in a high speed multi-stage compressor rig test: Isabe-2011-1223. In: *ISABE*, Gothenburg, Sweden, 2011.
5. Lapworth BL. Hydra-CFD: a framework for collaborative CFD development. In: *International conference on scientific and engineering computation IC-SEC,* Singapore, 2004.
6. Giles M. *Non-reflecting boundary conditions for the Euler equations*. CFDL-TR-88-1. Department of Aeronautics and Astronautics, Massachusetts Institute of Technology, Cambridge, MA, USA, 1988.
7. Schnell R, Voges M and Möning R. Investigation of blade tip interaction with casing treatment in a transonic compressor – part 2: numerical results: GT2008-50212. In: *ASME turbo expo,* Berlin, Germany, 2008.
8. Bölcs A and Suter P. *Transsonische Turbomaschinen. Wissenschaft und technik: Taschenausgaben*. Karlsruhe: G. Braun, 1986.
9. Schlechtriem S and Lötzerich M. Breakdown of tip leakage vortices in compressors at flow conditions close to stall: 97-GT-41. In: *ASME turbo expo,* Orlando, FL, USA, 1997.
10. Hathaway MD. *Passive endwall treatments for enhancing stability*. NASA TM 2007-214409. U.S. Army Research Laboratory, Glenn Research Center, Cleveland and Ohio and USA, 2007.
11. Madden DS and West MA. Effects of inlet distortion on the stability of an advanced military swept fan stage with casing treatment: GT2005-68693. In: *ASME turbo expo,* Reno-Tahoe, NV, USA, 2005.

Appendix

Notation

c_{ax}	axial velocity component (m/s)
$\|c\|$	absolute velocity magnitude (m/s)
max	maximum
$\dot{m}_{corr}$	corrected mass flow rate ($\mathrm{ms}\sqrt{\mathrm{K}}$)
num	numerical simulation
s	specific entropy (J/kgK)
α_2	absolute rotor outflow angle (measured against axial direction)
β_1	relative rotor inflow angle (measured against axial direction)
Δ	difference of two values
η_{poly}	polytropic efficiency
PE	peak efficiency
Π_t	total pressure ratio
ω	total pressure loss coefficient